Mon. Not. R. Astron. Soc. **000**, 1–?? (2021) Printed 27 September 2021 (MN LATEX style file v2.2)

Tidally tilted pulsation and mass transfer in the Algol-type system TZ Dra

F. Kahraman Aliçavuş[1,2⋆], G. Handler[3], F. Aliçavuş[1,2], P. De Cat[4], P. Lampens[4], Ö. Ekinci[1,2], D. Gümüş[5], F. Leone[6,7]

[1] *Çanakkale Onsekiz Mart University, Faculty of Sciences and Arts, Physics Department, 17100, Canakkale, Turkey*
[1] *Çanakkale Onsekiz Mart University, Astrophysics Research Center and Ulupınar Observatory, TR-17100, Çanakkale, Turkey*
[3] *Nicolaus Copernicus Astronomical Center, Bartycka 18, PL-00-716 Warsaw, Poland*
[4] *Royal Observatory of Belgium, Ringlaan 3, B-1180 Brussel, Belgium*
[5] *Istanbul University, Institute of Graduate Studies in Science,Programme of Astronomy and Space Sciences, 34116, Beyazıt,Istanbul, Turkey*
[6] *Dipartimento di Fisica e Astronomia, Sezione Astrofisica, Universita di Catania, Via S. Sofia 78, I-95123 Catania, Italy*
[7] *INAF, Osservatorio Astrofisico di Catania, Via S. Sofia 78, I-95123 Catania, Italy*

Accepted ... Received ...; in original form ...

ABSTRACT

Oscillating eclipsing Algols (oEAs) are remarkable systems to determine accurate fundamental stellar parameters (mass, radius) and probe the stellar interiors through pulsations. TZ Dra is an oEA system containing a δ Scuti component. To examine particular characteristics of such close systems including pulsations and mass transfer, we present a detailed photometric and spectroscopic study of TZ Dra. With the analysis of high-resolution spectra, the orbital parameters were determined by the radial velocity analysis and the atmospheric parameters were derived for the primary component. The binary modelling and the pulsational frequency analysis was carried out using the TESS data set. The Hα line profiles show the signature of mass transfer from the cool to the hot binary component. The conclusion of mass transfer/mass loss in the system was supported by the analysis of the orbital period changes. As a result, it was found that there is $3.52\text{x}10^{-10}$ $M_{\odot}$/year mass loss from the system most probably through the hotspot and stellar winds. Additionally, most pulsation frequencies originating from the primary component were found to be spaced by harmonics of the orbital frequencies in particular, twelve doublets spaced by $2f_{\rm orb}$ were detected from which we infer that this star a tidally tilted pulsator.

Key words: stars: binaries: eclipsing – stars: atmospheres – stars: fundamental parameters – stars: variables: δ Scuti – stars: individual: TZ Dra

1 INTRODUCTION

A significant fraction of stars in our galaxy is assumed to be a member of binary or multiple systems (Sana & Evans 2011; Alfonso-Garzón et al. 2014). A special group of binary systems is the eclipsing binaries. As the eclipsing binary stars are particular tools for the accurate determination of the fundamental stellar parameters such as mass (M) and radius (R), they are among the most studied stellar systems.

There are also some extremely spectacular eclipsing binaries that consist of at least one pulsating star. This kind of systems allows us to probe the stellar interiors through the study of pulsation frequencies occurring in the inner part of the oscillating binary component(s). Obtaining precise fundamental stellar parameters and having information about the stellar interior are certainly important and provides us with powerful tools to check the validity of present stellar structure models and compare evolutionary models for single stars and stars in binary systems. Therefore, most studies have been carried out about these objects for decades (e.g. Soydugan et al. 2016; Steindl, Zwintz, & Bowman 2021; Lampens 2021).

Different kinds of high and intermediate-mass main-sequence oscillating stars like β Cephei, δ Scuti and γ Doradus can be components of eclipsing binaries (Lampens 2021). However, the number of eclipsing binaries with δ

⋆ E-mail: filizkahraman01@gmail.com

Scuti components is the largest compared to other groups of main sequence pulsating stars (Kahraman Aliçavuş et al. 2017; Liakos & Niarchos 2017) because of their relatively shorter pulsation period and wide range of oscillation amplitude. The δ Scuti stars are $A-F$ type, dwarf to giant, pulsating variables which exhibit pulsations with frequencies higher than 5 d^{-1}. Their oscillations are thought to be excited by the κ mechanism operating in the He ionization zone (Houdek et al. 1999). The δ Scuti stars are located in the lower part of the classical Cepheid instability strip and they show pulsations in pressure (p) and gravity (g) modes which give information about the upper and lower parts of the stellar interior.

The first discoveries of δ Scuti stars in eclipsing binary systems were presented in the beginning of the 1970s (Tempesti 1971). Since that time, the number of known δ Scuti, stars in eclipsing binaries have been increased. The significant attempts to find the new candidates of this kind of systems was made by Mkrtichian et al. (2002, 2005); Soydugan et al. (2006). Soydugan et al. (2006) gave a list of possible candidates by searching for eclipsing binaries positioned inside the δ Scuti instability strip. Some new δ Scuti stars in eclipsing binaries were discovered by the investigation of the candidate stars given in this list (e.g. Sumter & Beaky 2007; Soydugan et al. 2008, 2011). The current number of the eclipsing binary δ Scuti stars is around 90 in the latest published catalog (Kahraman Aliçavuş et al. 2017). In recent years, this number is dramatically growing thanks to the high-precision data provided by the space telescopes such as CoRot, *Kepler* and TESS. In addition to revealing the new eclipsing binary δ Scuti stars, space telescopes also uncovered some new properties of these systems. For example, the first observational proof of δ Scuti type pulsations in only one hemisphere of the pulsating component of a close binary was discovered with TESS data (Handler et al. 2020). It was shown that in the close binary the oscillation axis of the pulsating binary component is aligned with the tidal axis and hence the star exhibit pulsations more effectively on its one hemisphere. After this discovery, two new systems showing similar behaviour were discovered (Kurtz et al. 2020; Rappaport et al. 2021). These variables are now dubbed "single-sided pulsators" (Handler et al. 2020) or, more general, tidally tilted pulsators (Fuller et al. 2020). As TESS observed almost the entire sky (Ricker et al. 2015), it has supplied sufficient data which help us to deeply understand the nature of stars like single-sided pulsators. TESS also observed a lot of known eclipsing binaries with δ Scuti stars which had only ground-based photometric data of much lower precision until now. One of these systems is TZ Dra.

TZ Dra is an eclipsing binary system with a spectral type of A7 V (Herbig 1960; Faulkner 1986). Its pulsational characteristic was first revealed by Mkrtichian et al. (2005). They found that the system exhibits ∼28 mins. oscillation and classified the primary (hot) binary component as a δ Scuti star. Pulsating stars in eclipsing Algols are called to be "oscillating Eclipsing Algol (oEA)" (Mkrtichian et al. 2004). TZ Dra is also an oEA system with an orbital period of 0.8660307 d (Kreiner 2004). The oEAs are substantial systems to trace the effects of mass transfer and/or mass loss to pulsations. In these Algol-type systems, mass is transferred from the evolved cool component to the pulsating hot component (Kopal 1955). It was shown that mass transfer affects the pulsations (Mkrtichian et al. 2004; Rodríguez et al. 2004). The effect of mass transfer in Algols can be revealed by following different features of the stellar spectra. Mass transfer can show itself as absorptions and/or emissions in Hα lines (Vesper, Honeycutt, & Hunt 2001; Soydugan et al. 2007). To investigate the effect/impact of mass transfer and/or mass loss on pulsations in oEA systems TZ Dra is a unique tool. Therefore, we performed a detailed analysis of TZ Dra using its high-quality TESS data in combination with newly acquired high-resolution spectra.

We organise the study as follows. In Sect.2, the information about the observational data is given. The radial velocity measurements and their analysis are introduced in Sect.3. In Sect.4 and 5, we present the spectral analysis and the binary modelling, respectively. The examination of the structure of the system's Hα line is given in Sect. 6. The orbital period changes and the time-series analysis are introduced in Sect.7 and 8, respectively. In the final section, Sect.9, discussion and conclusions are presented.

2 OBSERVATIONAL DATA

In our investigation, we used Transiting Exoplanet Survey (TESS) data and obtained high-resolution spectra for TZ Dra.

TESS originally was designed to identify new exoplanets in bright stars ($I_c < 13$). It was launched in April 2018 and until now TESS has observed almost 75% of the sky. The TESS data have been taken with 2-min short cadence (SC) and 30-min long cadence (LC) (Ricker et al. 2015). The TESS survey are separated into 26 sectors in which around 27-days data are gathered. The TESS data are released in the Barbara A. Mikulski Archive for Telescopes (MAST)[1]. For TZ Dra, only the LC data of sector 14 and SC data of sectors 25, 26 are available in the MAST. In this study, both LC and SC TESS data were used.

The spectroscopic data were obtained High Efficiency and Resolution Mercator Échelle spectrograph (HERMES). The HERMES spectrograph is attached to 1.2-m Mercator telescope at the Roque de los Muchachos observatory at La Palma, Spain. The spectrograph has a resolving power of 85000 and it provides spectra in a spectral range ranging from 377 to 900 nm (Raskin et al. 2011). For TZ Dra, we got 36 HERMES spectra which were collected between May and September 2020. The spectra were taken at different epochs to get spectra spread over the orbital periods of TZ Dra. The signal-to-noise (S/N) ratio of these spectra ranges from 60 to 100 and on average we have 83 S/N ratio.

In this study, the TESS photometric data and HERMES spectra were used for the radial velocity analysis, binary modelling, the determination of the atmospheric parameters such as effective temperature ($T_{\rm eff}$), surface gravity ($\log g$), microturbulence velocity (ξ) and also projected rotational velocity ($v \sin i$) of the system and time-series analysis.

[1] https://mast.stsci.edu

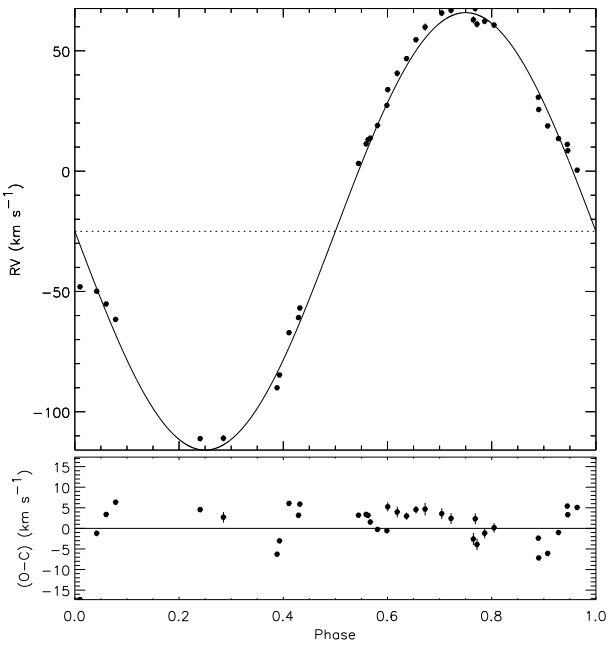

Figure 1. Upper panel: Theoretical (solid line) fit to the v_r mesurements (dots). Lower panel: residuals.

3 RADIAL VELOCITY ANALYSIS

To accurately determine the fundamental stellar parameters of system, binary modelling should be done with the radial velocity (v_r) measurements in addition to photometric data. Therefore, before performing the binary modelling we obtained the v_r data of the binary components. In this study, to measure the v_r values we used a synthetic spectrum that generated considering the spectral type of TZ Dra. The v_r values were obtained utilizing the FXCOR task of IRAF[2] package program(Tody 1986). This task uses the cross-correlation technique to measure v_r values. As a result of our analysis, we did not find the contribution of the secondary component in the spectra and only measured the v_r values of the primary component. The resulting v_r measurements are listed in Table A1.

The v_r analysis was carried out using the `rvfit` code [3] which is suitable for the v_r analysis of single and double-lined binary systems. In this analysis, we fixed the orbital period of the system as 0.8660307 days (Kreiner 2004). The periastron passage time (T_o), the velocity of mass centre (V_γ), the amplitude of the v_r curve (K), argument of periastron (ω), orbital eccentricity (e) and the projected semi-major axis (asin$i$) parameters were searched for during the analysis. As the e value was found to be 0 in the first a few iterations, this value and also the ω parameter were assumed to be 0 and 90 degree respectively in the further analysis. In conclusion, we obtained the orbital parameters and they are given in Table 1. The best theoretical v_r fit to the v_r measurements is shown in Fig.1.

[2] http://iraf.noao.edu/
[3] http://www.cefca.es/people/riglesias/rvfit.html

Table 1. The results of the radial velocity analysis. [a] represents the fixed parameters.

Parameters	Value
P (d)	0.8660310^a
T_0 (HJD)	2452500.63606 ± 0.00004
e	0.0^a
ω (deg)	90^a
γ (km/s)	-25.02 ± 0.11
K_1 (km/s)	90.90 ± 0.20
$a_1 \sin i$ ($R_\odot$)	1.555 ± 0.003
$f(m_1, m_2)$ ($M_\odot$)	0.0674 ± 0.0004

4 SPECTRAL ANALYSIS

In our radial-velocity analysis, no evidence of the cool (secondary) component spectrum was found in the cross-correlation function. Therefore, in our spectral analysis, we determined only the atmospheric parameters of the hot (primary) component. In any case, we used the spectra taken at close to 0.5 orbital phase where the secondary component is partically covered by the primary. In this way, we decreased the possible effect of the secondary component in the spectra. Three spectra at ∼0.5 phase were chosen and combined to achieve a higher S/N ratio (∼165) spectrum.

Using the combined spectrum, we first determined the initial $T_{\rm eff}$ value from the hydrogen line modelling. In this and next spectral analysis, the plane-parallel, hydrostatic, local thermodynamic equilibrium (LTE) ATLAS9 atmosphere models (Kurucz 1993) were used and the theoretical spectra were generated by using the SYNTHE code (Kurucz & Avrett 1981). In the hydrogen line analysis, we assumed solar abundance and fixed the $\log g$ as 4.0 dex. These assumptions were done because the profile of the hydrogen lines is not affected by the metallicity and for the stars cooler than 8000 K there is a negligibly weak dependence to $\log g$ (Smalley et al. 2002; Smalley 2005). Additionally, in the hydrogen line analysis, we only used Hδ and Hγ lines because it is known that in Algol type systems due to the mass transfer effect there could be absorption and/or emission seen in Hα and Hβ lines (Vesper, Honeycutt, & Hunt 2001; Soydugan et al. 2007). Those extra features in hydrogen lines can be analysed after subtracting the theoretical hydrogen line profile. This examination is presented in Sect. 6.

In the hydrogen line analysis, several synthetic spectra were generated for a range of $T_{\rm eff}$ ($\sim 7000-8500$ K) in 100 K steps and they were fitted to the observed hydrogen lines. The best fit theoretical spectra were found considering the minimum χ^2 value (for more detail see Catanzaro, Leone, & Dall (2004)). As a result of the analysis, we found the hydrogen $T_{\rm eff}$ values as 7700 ± 250 K and the consistency of the theoretical hydrogen lines with the observations is demonstrated in Fig. 2.

To derive the $\log g$, ξ values and improve the $T_{\rm eff}$, we used the excitation/ionization-abundance relations which rely on the Boltzman and Saha equations. Taking into account the hydrogen-based $T_{\rm eff}$ we decided to use iron (Fe) lines because of its significant number at around this $T_{\rm eff}$. The method used in Kahraman Aliçavuş et al. (2016) was applied in the same way in this study. First, the Fe lines were

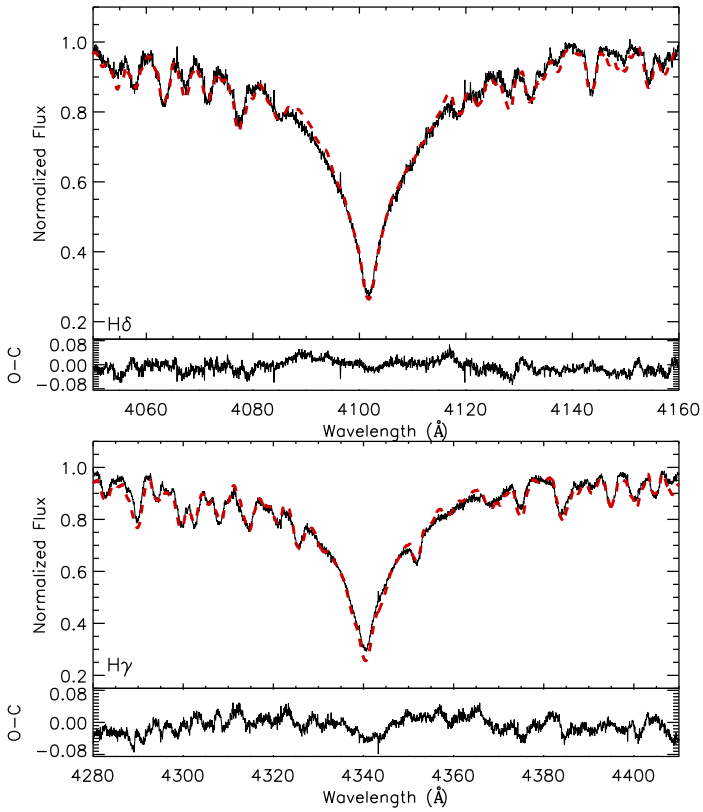

Figure 2. Theoretical hydrogen line fit (dashed line) to the observed Hδ and Hγ lines. The differences between the observed (O) and calculated (C) spectra are shown below of each panels.

Table 2. The final atmospheric parameters and $v \sin i$ value of the hot (primary) component star of TZ Dra.

$T_{\rm eff}$ (K)	$\log g$ (cgs)	ξ (km s^{-1})	$v \sin i$ (km s^{-1})
8100 ± 200	4.1 ± 0.2	1.9 ± 0.3	85 ± 3

chosen from the line list of Kurucz[4] and their corresponding abundances were derived for a $T_{\rm eff}$ $\log g$, and ξ range in a step of 100 K, 0.1 dex, and 0.1 km s^{-1}, respectively. The spectrum synthesis method was used in the analysis. It is known that for the correct atmospheric parameters, for different excitation/ionization potential one should get the same abundances as described by Kahraman Aliçavuş et al. (2016). In this way, the atmospheric parameters of the hot (primary) component of TZ Dra were obtained. The derived parameters is given in Table 2.

After we determined the atmospheric parameters, we derived the chemical abundances by taking these parameters as input and using the Kurucz line list. In this analysis, the abundances of the individual elements were adjusted until the minimum difference between the calculated and observed spectra was found. During this analysis, the $v \sin i$ parameter was also searched for. The abundances of the chemical elements are listed in Table 3, while the $v \sin i$ is given in Table 2. The chemical abundances distribution is

[4] kurucz.harvard.edu/linelists.html

Table 3. Abundances of individual elements of the primary star and Sun (Asplund et al. 2009). Number of the analysed spectral lines is given in the brackets.

Elements	Star abundance	Solar abundance
$_{6}$C	8.63 ± 0.45 (1)	8.43 ± 0.05
$_{12}$Mg	7.98 ± 0.40 (4)	7.60 ± 0.04
$_{14}$Si	6.97 ± 0.36 (5)	7.51 ± 0.03
$_{20}$Ca	6.48 ± 0.31 (6)	6.34 ± 0.04
$_{21}$Sc	3.37 ± 0.41 (3)	3.15 ± 0.04
$_{22}$Ti	4.91 ± 0.34 (17)	4.95 ± 0.05
$_{23}$V	4.15 ± 0.42 (2)	3.93 ± 0.08
$_{24}$Cr	5.57 ± 0.35 (10)	5.64 ± 0.04
$_{25}$Mn	5.02 ± 0.33 (5)	5.43 ± 0.05
$_{26}$Fe	7.37 ± 0.21 (40)	7.50 ± 0.04
$_{28}$Ni	6.18 ± 0.38 (5)	6.22 ± 0.04
$_{38}$Sr	2.71 ± 0.45 (1)	2.87 ± 0.07
$_{56}$Ba	2.39 ± 0.42 (2)	2.18 ± 0.07

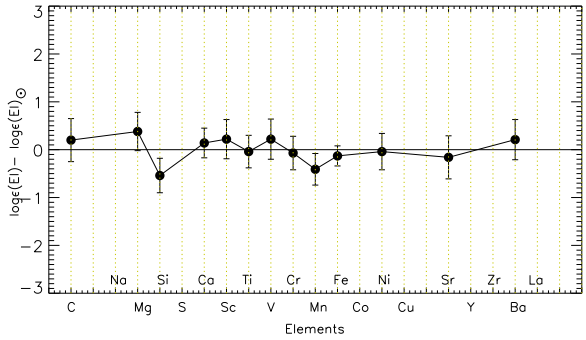

Figure 3. The chemical abundance distribution of the primary component of TZ Dra. The solar abundance was taken from Asplund et al. (2009).

also illustrated in Fig. 3. The consistency between the resulting synthetic and the observed combined spectrum is shown in Fig.4.

The errors in the atmospheric parameters were estimated considering the 5% difference in the used relations in the atmospheric parameters determination analysis. Additionally, the uncertainties in the chemical abundances were calculated taking into account the effects of the errors in the input parameters and S/N ratio as described by Kahraman Aliçavuş et al. (2016).

5 BINARY MODELLING

In order to derive the orbital and the fundamental stellar parameters of TZ Dra, we modelled the binary light curve. First, whole available TESS data were taken into account to control whether it changes from one sector to other. Because of a possible spot existence the maximum points of the binary light curve could differ from one sector to other. No significant variation was found in this examination. Therefore, in the binary modelling we used only one sector (25) data.

The pulsations of the pulsating component do not

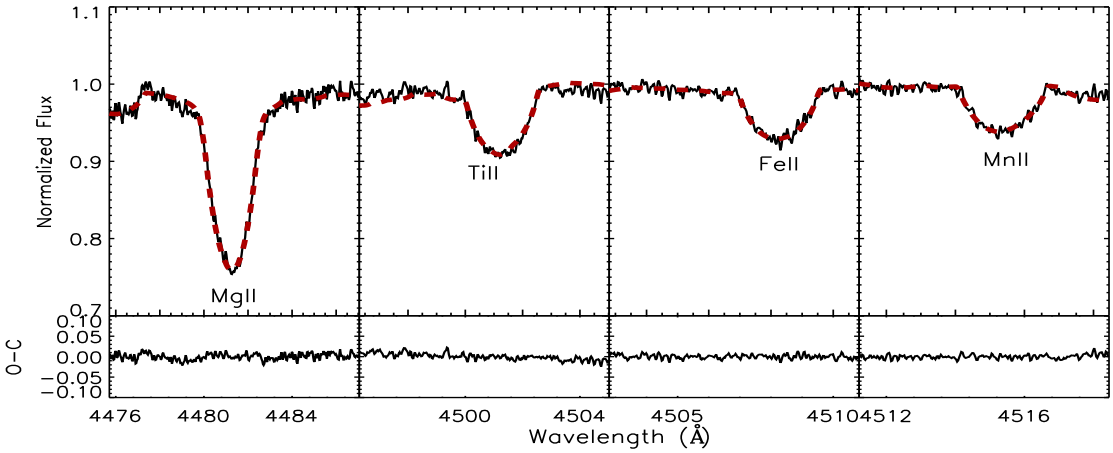

Figure 4. Consistency between the synthetic (dashed lines) and the observed spectra.

deeply affect the orbital/geometrical variation of TZ Dra. However, we removed the dominant pulsations from the light curve by performing a preliminary Fourier analysis with PERIOD04 (Lenz & Breger 2005). The remaining data were first phased, normalised and then binned to make them usable for the binary modelling with the code of Wilson-Devinney (Wilson & Devinney 1971).

In this analysis, we used the findings of the previous binary modelling (Liakos & Niarchos 2013) as input. Only the $T_{\rm eff}$ value of the primary component and the results of the v_r analysis (γ, e, a) were taken from our study and they were fixed during the analysis. The $T_{\rm eff}$ value of the primary star was found slightly different in two different approaches. Therefore, in this analysis, we used the average $T_{\rm eff}$ (7900 K) as input. The other fixed parameters are bolometric albedos (Ruciński 1969), bolometric gravity-darkening coefficient (von Zeipel 1924), and logarithmic limb darkening coefficient (van Hamme 1993). The TESS passband is not included to the Wilson-Devinney code, therefore, the I-band was assumed in the binary modelling as the TESS passband is centered at Cousins I-band. The fixed coefficients were also chosen considering the I-band. Those coefficients were taken with the the same way as given Kahraman Aliçavuş & Aliçavuş (2019). The $T_{\rm eff}$ of the cool component, phase shift (ϕ), orbital inclination (i), the mass ratio (q=M_{hot}/M_{cool}), fractional luminosities and the dimensionless potential (Ω) of binary components were searched for. During the analysis, a synchronous rotation and a semi-detached binary configuration were assumed as the system defined a semi-detached binary before (Liakos & Niarchos 2013). The Wilson-Devinney code combined with Monte-Carlo simulation was used in the binary modelling (Zola et al. 2004, 2010).

As the system was found to be a single-lined binary, there is no certain information about the q value. Therefore, a q search was carried out by checking the minimum χ^2 value. Consequently, it was found that the q value should be around 0.42 ± 0.03. The q search is shown in Fig. A1. The binary modelling was started adopting q value input. In the first binary modelling steps we noticed that in the non-eclipsing light curve there are some asymmetries which are probably caused by a star spot(s). Therefore, we included star-spot modelling in our analysis as well. As a result of this

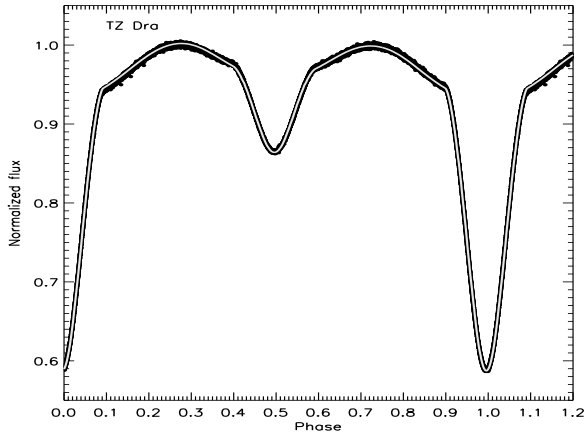

Figure 5. Theoretical binary modelling fit (solid line) to the TESS light curve of TZ Dra.

analysis, we found the best fitting model with a hot spot on the primary star. The results of the binary modelling are listed in Table 4 and the best fitting theoretical model to the TESS data is illustrated in Fig. 5. The Roche lobe geometry of the system with the hot spot on primary's surface is shown in Fig.6

The fundamental stellar parameters such as M, R, luminosity (L), bolometric magnitude ($M_{bolometric}$), absolute magnitude (M_V) and also $\log g$ parameters for both binary components were calculated using the mass function f found in the v_r analysis, the well-known Kepler and Pogson equations. These parameters are also listed in Table 4.

6 Hα LINE PROFILE AND MASS TRANSFER EXAMINATION

Algols are semi-detached, close, short-period binary systems that consist of a hot (B-A) main-sequence and a cooler, less massive evolved component. This evolved cooler component fills its Roche lobe and transfers mass from Roche lobe overflow (Kopal 1955). The mass transfer can be noticed from some additional features affecting the photometric and spec-

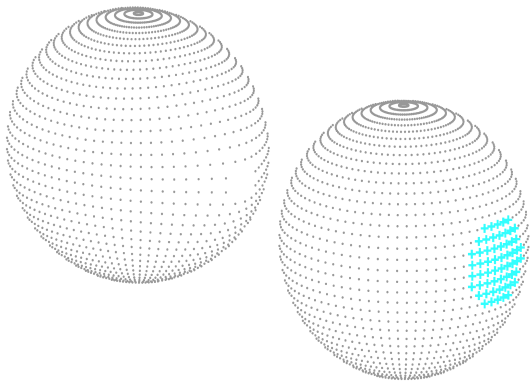

Figure 6. Roche geometry of TZ Dra at around 0.6 phase. Blue spot on the primary star represents the hot-spot.

Table 4. Results of the light curve analysis and the fundamental stellar parameters. The Subscripts 1, 2 and 3 represent the primary, the secondary, and third binary components, respectively. [a] Shows the Fixed Parameters.

Parameter	Value
i (^{o})	75.138 ± 0.015
T_1[a] (K)	7900 ± 250
T_2 (K)	4970 ± 233
Ω_1	3.848 ± 0.046
Ω_2	2.734 ± 0.035
Phase shift	-0.0044 ± 0.0001
q	0.428 ± 0.013
r_1* (mean)	0.2953 ± 0.0036
r_2* (mean)	0.3070 ± 0.0026
l_1 / (l_1+l_2)	0.787 ± 0.016
l_2 /(l_1+l_2)	0.213 ± 0.016
l_3	0.0
Spot Parameters	
Co-Latitude (deg)	90[a]
Longitude (deg)	190.84± 0.14
Radius (deg)	19.53±0.04
Temperature Factor**	1.052±0.012
Derived Quantities	
M_1 ($M_\odot$)	2.039 ± 0.004
M_2 ($M_\odot$)	0.872 ± 0.003
R_1 ($R_\odot$)	1.611 ± 0.052
R_2 ($R_\odot$)	1.675 ± 0.038
log ($L_1/L_\odot$)	0.960 ± 0.033
log ($L_2/L_\odot$)	0.188 ± 0.054
log g_1 (cgs)	4.30 ± 0.02
log g_2 (cgs)	3.92 ± 0.03
$M_{bolometric1}$ (mag)	2.34 ± 0.07
$M_{bolometric2}$ (mag)	4.27 ± 0.08
M_{V1} (mag)	2.32 ± 0.09
M_{V2} (mag)	4.50 ± 0.13
M_{TESS1} (mag)	2.35 ± 0.05
M_{TESS2} (mag)	3.77 ± 0.09

* fractional radii, ** $T_{\rm eff}$ spot/$T_{\rm eff}$ star

troscopic data. The effect of mass transfer in Algols shows itself especially as distortions in the v_r data of the primary component, and additional emission and/or absorption in Hα and Hβ lines (Vesper, Honeycutt, & Hunt 2001; Soydugan et al. 2007). When the v_r curve, Hα and Hβ line profiles of TZ Dra were examined, we noticed a distortion in the v_r data and significantly different profile in Hα. These additional absorption and/or emission lines in Hα are signs of mass transfer occurring in Algol type systems. As explained by Vesper, Honeycutt, & Hunt (2001), emissions are happened by stream-disk or star-stream interaction in a region between binary components. Absorption lines are also originated from the matter around the primary component or "stream projected against primary" (Vesper, Honeycutt, & Hunt 2001). So the existence of these absorption and emission profiles in Hα gives us information about the mass transfer. Therefore, we extracted the Hα line profiles of TZ Dra. The best fit theoretical atmosphere model obtained in the analysis of the hydrogen lines was used in this analysis. This atmosphere model was fitted to the Hα profiles and then it was extracted from the observed Hα lines. In this way, the profiles of absorption and emission lines were obtained as shown in Fig.7. In these residual spectra, we found one emission and two absorption line profiles. The v_r changes of these lines were measured and the variation of them according to the orbital phase were obtained as shown in Fig. 8. When the v_r variation of these lines were examined, we noticed that the emission profiles caused by the star-stream or star-disk interaction between two stars. Because these interactions create emission lines and they are visible at around near quadrature phases as obtained in this study (Vesper, Honeycutt, & Hunt 2001). The absorption line 1 (see Fig.7 and Fig.8) is thought to be due to the stream projected against the primary component. In this case, absorption lines are observed near primary eclipse ingress or egress (Vesper, Honeycutt, & Hunt 2001) as we obtained for absorption line 1. Additionally, the v_r variations of this line follows the v_r profiles of the primary component. The other absorption line (line 2) seems to follow the secondary component and there is no explanation for this kind of absorption line profile occurring in Algol type systems. This line thought to may be caused by the mass stream from the secondary component. It only detected around the primary eclipse as can be seen from Fig.8. As a result, with this investigation, we showed the mass transfer signature of TZ Dra.

7 ORBITAL PERIOD VARIATION

Mass transfer and mass loss in a system can be evidenced by an orbital period variation analysis as well. Hence, to search for the mass loss in TZ Dra, we also studied the orbital period changes. All available literature minima times of TZ Dra were collected from the O-C Gateway[5]. Additionaly, we used TESS data to calculate new minima times. In this calculation, only the SC data were used because the minimum light variations were more clear in these data and that makes to measure minima times easy. We measured

[5] http://var2.astro.cz/ocgate/

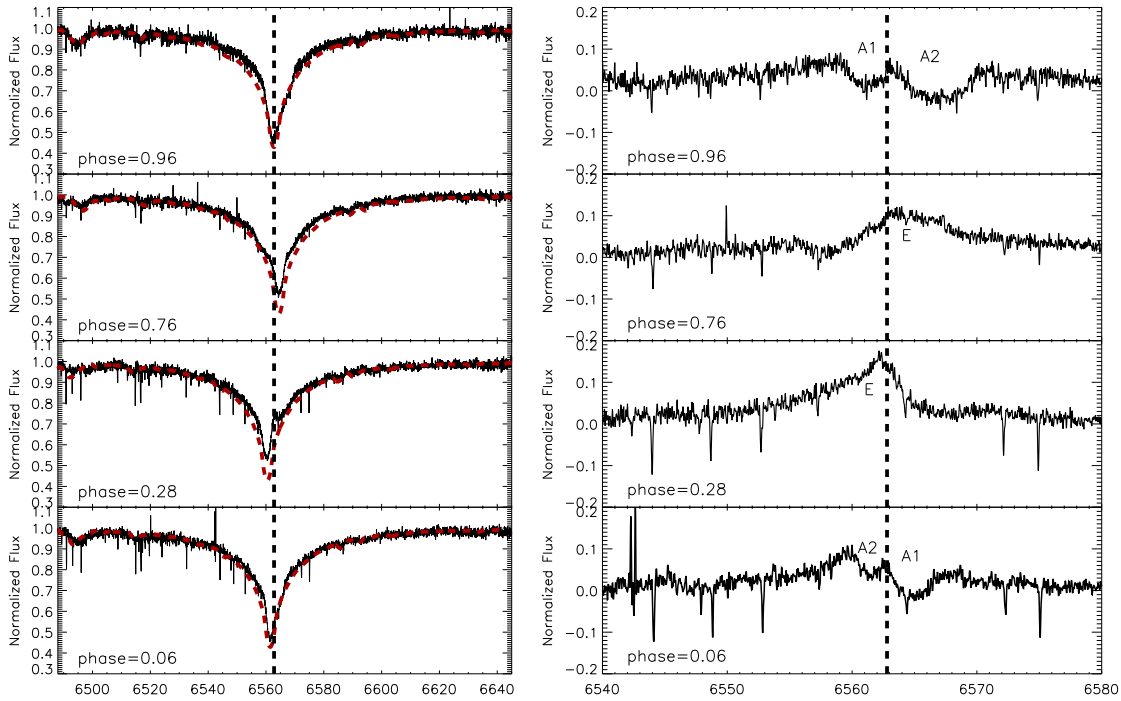

Figure 7. The Hα profiles at different orbital phases (left panels) and the residuals (right panels) from the observed and the theoretical Hα (red dashed lines) profiles shown in the left panels. The vertical dashed lines represent the laboratory wavelength of Hα. The abbreviations A1, A2 and E show absorption 1, absorption 2 and emission lines seen in the residuals.

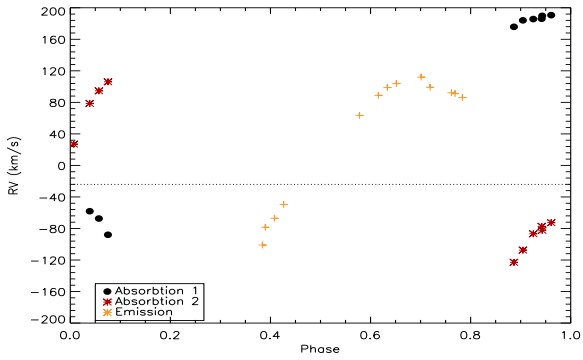

Figure 8. The radial velocity variations of the absorption and emission lines shown in Fig. 7.

three primary and secondary minima times from each sector and in total 12 new minima times were derived from the TESS observations. To obtain a new minima time a photometric observation was carried out at the Çanakkale Onsekiz Mart Observatory with IST60 telescope (60-cm). The minima times from the TESS and new photometric observation were calculated using the method of Kwee & van Woerden (1956). All the minima times are listed in Table A2. To increase the sensitivity of our orbital-period variation (O-C) analysis, in addition to TESS and new minima times, we used only the literature CCD and photoelectric minima times in the analysis. In total, 16 photoelectric and 67 CDD minima times were used. During the analysis, data weights were taken as 3 for photoelectric data and 10 for CCD the minimas and the weighted least squares method was used (Zasche et al. 2009).

When we examined the O-C diagram of TZ Dra, we found a parabolic variation combined with another periodic change. First a parabolic fit was applied to the O-C data. As a result, the quadratic term (Q) was found to be -1.3265x10^{-10} and a quadratic ephemeris was obtained as follows:

$$HJD(MinI) = 2452500.6419(5) + 0.8660316(8) \,.\, E$$

$$- 1.3265 \,.\, 10^{-10}(3) \,.\, E^2(1)$$

The parabolic variations in the O-C diagram could be caused by mass transfer between the binary component and/or mass loss from the system. For TZ Dra a 0.009 s/year decrease in the orbital period was obtained as given in Table 5. This shows us that the mass loss is effective in TZ Dra.

After removing the parabolic fit from the O-C data, we obtained another variation in the residuals. For the variation in the residual O-C diagram the light-time effect (LITE) caused by a third body orbiting around the centre of mass (e.g. Pribulla et al. 2005; Erdem et al. 2011) was tested. The physical relation between the O-C and LITE was formalised by Irwin (1959). Irwin (1959) described the time delay (ΔT) in the period with the semi-major axis (a), speed of light (c), i, e, true anomaly (υ) and longitude of periastron (w). The best theoretical fit representing this variation in the O-C diagram is obtained by the following equation:

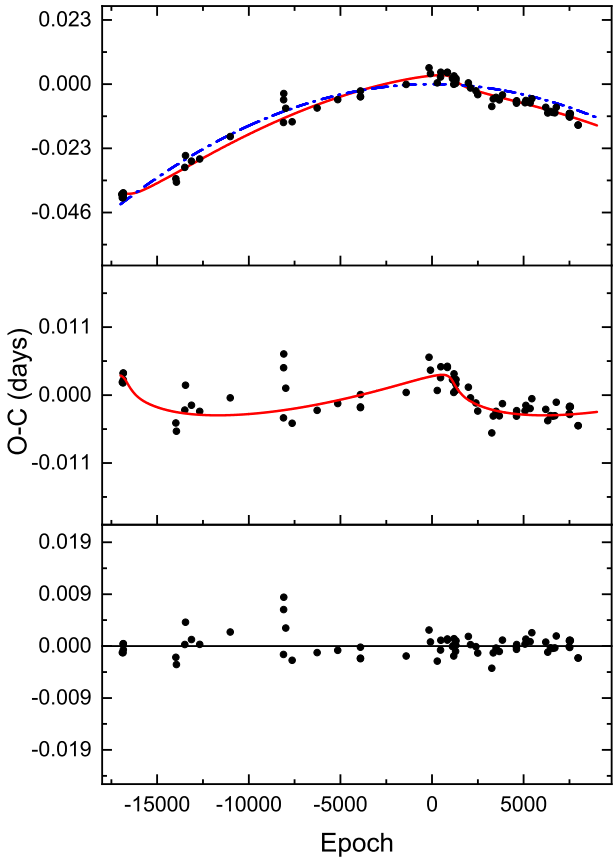

Figure 9. The theoretical fits to the O-C data. Upper panel shows the both parabolic (blue dashed line) and the parabolic and LITE model fit (red). Middle and lower panels illustrate the only LITE fit and the residuals from the combined fit, respectively.

$$HJD(MinI) = 2452500.6419(5) + 0.8660316(8) \,.\, E$$
$$- 1.3265 \,.\, 10^{-10}(3) \,.\, E^2 + \Delta T(2)$$

As a result, in the system we found a third component with a 45.8-year orbital period and a maximum mass of 0.17 ± 0.03 M⊙ if it has an orbital inclination of 90^o. This third component could not found in the binary modeling because of it is relatively small mass. The results of the O-C analyses for the parabolic and LITE variations and the combined best theoretical fit to the observations are given in Table 5 and the best theoretical O-C fit to the observation points is shown in Fig. 9. respectively.

8 TIME-SERIES ANALYSIS

8.1 Mean binary light curve

To perform a frequency analysis of pulsating components of eclipsing binary stars, it is often advantageous to remove the mean binarity-induced light curve by phenomenological fit instead of a physical model. In that way, possible

Table 5. The results of the O-C diagram analysis. A and subscript 3 represent the amplitude of LITE and third body.

Parameter	Value
T_o (HJD)	2452500.6419 ± 0.0005
P (day)	$0.86603164 \pm 0.00000008$
Q (day). (10^{-10})	-1.3265 ± 0.0003
dP/dT (s/year)	-0.009 ± 0.001
dM/dt ($M_\odot$/year). 10^{-9}	-3.52 ± 0.24
P_3 (year)	45.82 ± 0.90
$a_3 \sin i$ (AU)	0.98 ± 0.09
A_s (day)	0.0032 ± 0.0004
e_3	0.83 ± 0.05
ω_3 (degree)	170 ± 7
f (m_3) ($M_\odot$)	0.0005 ± 0.0001
m_3 ($M_\odot$) (i=90)	0.17 ± 0.03

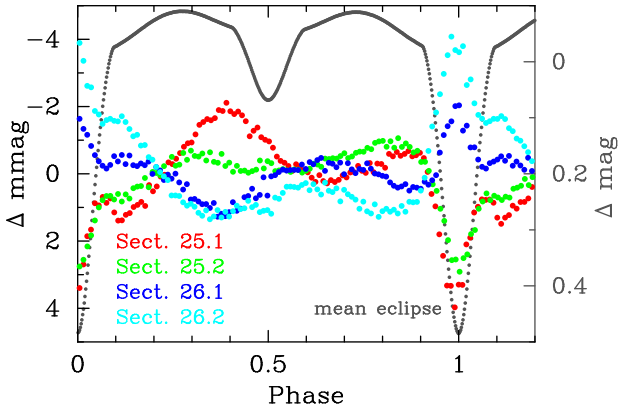

Figure 10. The mean *TESS* light curve of TZ Dra and the temporal variations of the deviations from the mean (in bins of 0.01 in phase and magnified by a factor of 60).

imperfections in a model fit cannot generate spurious periodic signals that can be mistaken for pulsation frequencies. In that spirit, we computed a 100-harmonic fit to the light curve based on the orbital frequency derived to be 1.1547060 ± 0.0000004 d^{-1} from the *TESS* photometry alone which is quite similar to value derived from orbital period analysis and removed it before embarking on frequency analysis.

Figure 10 compares the mean light curve of TZ Dra as derived from the *TESS* Sector 25 and 26 2-min cadence photometry with the residuals left behind subtracting this mean light curve from the mean computed for two halves of each sector. The strongest changes occur at primary minimum, which may at first glance suggest different contamination from neighboring stars in the photometric aperture, as the target was placed on different CCDs throughout the different sectors (the contamination factor for the star in the TESS Input Catalog (Stassun et al. 2019) is 0.0334). However, the *absence* of such changes near secondary minimum and that they occur continuously as far as we can judge argues that these variations are real. They could be caused by the circumbinary matter around the primary component. In any case, the residuals left behind subtracting the mean binary

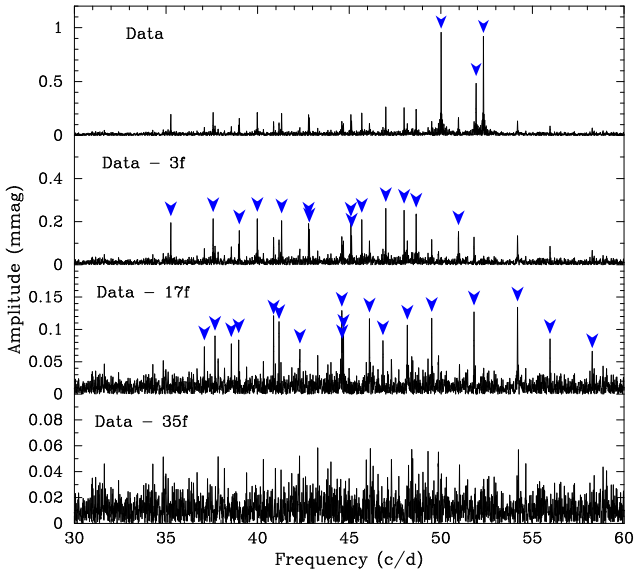

Figure 11. The Fourier Transform of the residual *TESS* light curve of TZ Dra after filtering the binarity-induced light variations (top) and subsequent prewhitening steps. The blue arrows denote the signals detected.

light curve do not generate signals in the frequency domain relevant for pulsational variability.

8.2 Pulsational frequency analysis

The residuals after the fit were searched for frequencies of pulsation using the Period04 software (Lenz & Breger 2005). This package applies single-frequency power spectrum analysis and simultaneous multi-frequency sine-wave fitting. It also includes advanced options such as the calculation of optimal light-curve fits for multiperiodic signals including harmonic, combination, and equally spaced frequencies. These sine-wave fits are subtracted from the data and the residuals examined for the presence of further periodicities. The application of this procedure, called prewhitening, to TZ Dra is illustrated in Fig. 11.

To decide whether or not a periodic signal in a time series is statistically significant or not, several criteria have been proposed, the most commonly used probably the one by Breger et al. (1993). This criterion states that a given peak must exceed the mean amplitude in the Fourier spectrum by a factor of 4 in the local frequency domain to be considered significant. For space-based data, this can however lead to an overinterpretation of the periodic content (Balona 2014). Consequently, we have stopped the frequency search after the detection of 35 pulsational signals to err on the side of caution; the strongest residual peak in the lowest panels of Fig. 11 has an amplitude S/N ratio of 5.2.

During the frequency analysis it became clear that many of the pulsational signals are spaced by integer multiples of the orbital frequency ν_{orb} from other pulsation frequencies. We therefore demanded that Period04 would fix those frequencies to exactly the predicted value as the orbital frequency is determined to considerably higher precision than the individual pulsation frequencies. We list the frequency solution so derived in Table 6, where we also quote formal errors on the derived parameters following Montgomery & Odonoghue (1999).

Table 6. A least squares fit of the pulsation frequencies of TZ Dra. The zero point for the phases, $t_0 = 2459008.8585$, has been chosen to be at a time of primary eclipse. Error estimates for the independent frequencies and phases are given in braces in units of the last digits after the comma.

	frequency d^{-1}	amplitude mmag ±0.012	phase radians
ν_1	50.0174(1)	0.950	4.51(1)
$\nu_1 + 2\nu_{orb}$	52.3268(1)	0.910	1.35(1)
ν_2	51.9264(2)	0.467	0.83(2)
$\nu_3 - 2\nu_{orb}$	44.6863(12)	0.092	1.84(11)
ν_3	46.9957(4)	0.264	4.95(4)
$\nu_4 - \nu_{orb}$	45.6875(5)	0.212	3.73(5)
ν_4	46.8422(13)	0.082	3.42(12)
$\nu_4 + \nu_{orb}$	47.9969(4)	0.254	3.73(4)
ν_5	48.6545(5)	0.235	4.91(4)
$\nu_5 + 2\nu_{orb}$	50.9639(7)	0.154	1.88(7)
ν_6	37.5715(5)	0.218	3.16(5)
$\nu_6 - 2\nu_{orb}$	35.2621(6)	0.195	3.06(5)
ν_7	41.3112(5)	0.207	4.71(5)
$\nu_7 - 2\nu_{orb}$	39.0018(7)	0.149	4.86(7)
ν_8	39.9832(5)	0.214	6.26(5)
$\nu_8 - 2\nu_{orb}$	37.6738(12)	0.089	3.00(11)
ν_9	45.0894(6)	0.194	1.75(5)
$\nu_9 - 2\nu_{orb}$	42.7800(6)	0.190	4.88(5)
ν_{10}	42.8204(7)	0.167	2.88(6)
$\nu_{10} + 2\nu_{orb}$	45.1298(8)	0.139	6.15(7)
ν_{11}	51.8128(9)	0.128	4.10(8)
$\nu_{11} - 2\nu_{orb}$	49.5034(9)	0.118	4.21(9)
ν_{12}	54.1882(8)	0.134	4.86(8)
$\nu_{12} - 7\nu_{orb}$	46.1053(9)	0.117	1.66(9)
ν_{13}	40.8723(10)	0.114	4.03(9)
$\nu_{13} - 2\nu_{orb}$	38.5629(14)	0.079	4.25(13)
ν_{14}	58.2668(18)	0.062	2.87(16)
$\nu_{14} - 2\nu_{orb}$	55.9574(13)	0.084	5.81(12)
ν_{15}	44.6175(14)	0.076	3.90(13)
$\nu_{15} - 2\nu_{orb}$	42.3081(16)	0.069	4.14(15)
ν_{16}	44.5955(9)	0.126	2.23(8)
ν_{17}	41.1696(10)	0.107	2.44(10)
ν_{18}	48.1700(10)	0.106	4.19(10)
ν_{19}	38.9667(13)	0.085	2.53(12)
ν_{20}	37.0940(15)	0.074	1.21(14)

The pulsation frequencies determined this way range from $35.26 - 58.27$ d^{-1}. From the mass and radius for the primary δ Scuti pulsator, one can derive pulsation "constants" $Q_i = P_i\sqrt{(\rho/\rho_\odot)}$ [6] between $0.012 - 0.020$ d. This corresponds to pulsation in relatively high-order p modes in the range of the second to fifth radial overtone (Fitch 1981) which, in combination with the relatively unevolved state of the pulsator, suggests a pulsation spectrum containing few mixed modes.

Fourteen out of the 20 independent pulsation frequencies detected for TZ Dra occur in multiplets. Twelve of those are doublets spaced by twice the orbital frequency, one is a triplet with a weak centroid spaced by the orbital frequency. With one exception, all of the single frequencies are low in

[6] P_i: Period of the used frequency

amplitude, so it is possible that they have undetected multiplet companions. Furthermore, many of the doublet components are fairly similar in amplitude, and all of them are, within the errors, either in phase or π rad out of phase at primary minimum.

These are signatures of tidally tilted pulsation. Reed, Brondel, & Kawaler (2005) have shown how the oscillation spectrum of a single mode of given spherical degree l and azimuthal order m becomes modified due to the varying aspect of the pulsation axis over the orbital cycle. In brief, a single frequency splits up into multiplets determined by the type of mode, and by the inclination of the pulsational and rotational axes. These multiplets are spaced by integer multiples of the orbital frequency. This is what is seen here. The frequency doublets in our case thus are parts of multiplets centred on the frequency average of the two components. In Fig.12 we show the behaviour of the amplitudes and phases of a few selected modes over the orbit.

The amplitude of the ν_1 doublet is at maximum near quadrature, and reaches almost zero near primary and secondary eclipse, respectively. The zero-crossing means that a node line of a nonradial pulsation mode crosses the line of sight. Assuming that the pulsational axis lies in the orbital plane (there would be no amplitude modulation if it was aligned with the rotational axis which we assume to be normal to the orbital plane), this must therefore be a sectoral mode. The singlet ν_2 shows no phase modulation over the orbital cycle and almost no amplitude variation, except near primary eclipse. This would at first sight imply a radial mode. However, in that case one would expect the pulsation amplitude to decrease near primary eclipse, when part of the pulsating star is covered by the cooler companion that, at this orbital phase, contributes relatively more to the total flux observed. That this is not the case implies that ν_2 is also due to a nonradial mode, and that the increase in amplitude during primary eclipse is due to part of the surface that causes geometrical cancellation (Dziembowski 1977) being covered by the companion. The mode triplet ν_4 and the doublet including ν_6 behave similarly: they have highest amplitude at primary and secondary eclipse, respectively, but an amplitude close to zero near quadrature. They are therefore tidally tilted axisymmetric modes.

Which of the mode doublets correspond to axisymmetric and sectoral modes, respectively, can be directly read off Table 6. The multiplets that are in phase at primary minimum (triplet ν_4 and the doublets containing ν_6, ν_7, ν_{11}, ν_{13} and ν_{15}) are the $m = 0$ modes and the doublets π rad out of phase (ν_1, ν_3, ν_5, ν_8, ν_9, ν_{10}, ν_{12} and ν_{14}) are sectoral modes. It is interesting to note that the centroid frequencies of the doublets containing axisymmetric modes are fairly equally spaced in frequency and may imply a mean frequency spacing of about 7.1 d^{-1} for consecutive radial orders of modes of the same l, which is close to the expected value of a star with the parameters of the primary of TZ Dra listed in Table 4. Whereas a detailed seismic study of the pulsating component of TZ Dra is out of the scope of the present paper, and will need proper consideration of the tidal distortion of the oscillations (cf. Fuller et al. 2020) and the altered stellar structure due to ongoing mass transfer (e.g., Miszuda, Szewczuk, & Daszyńska-Daszkiewicz 2021), let it suffice to say that this is a very interesting system for more in-depth theoretical modelling.

In comparison to the remaining pulsational mode structure of TZ Dra, the frequency doublet ν_{12} and $\nu_{12} - 7\nu_{orb}$ appears to be an "outlier". Perhaps the frequency match is just a numerical agreement, but in that case there would be little reason why the phases of those two signals are also π rad out of phase. This is a hint that these two signals are generated by the same pulsation mode, which then must however be $l > 3$.

9 DISCUSSION AND CONCLUSIONS

In this study, we present the results of the spectroscopic and TESS photometric examinations of TZ Dra. Using the high-resolution spectra, we measured the radial velocities of primary component and found no significant signal from the cool (secondary) component. Therefore, the spectral analysis was carried out only for the hot (primary) component. The TESS photometric data were used in the binary modelling and pulsational frequency analysis.

The first binary modeling of the system was performed by Liakos & Niarchos (2013). Since they used ground-based photometric data in their analysis, there are significant differences between the results of our binary modelling and theirs because of the sensitivity difference between the TESS and ground-based data. The i and q values show significant discrepancy, as a result the fundamental stellar parameters obtained in this study are quite different than the findings of Liakos & Niarchos (2013). Additionally, in their analysis, no spot variation was found in the light curve. Thanks to the spectroscopic data and high-quality TESS data the fundamental stellar parameters for TZ Dra system were determined precisely.

TZ Dra is an Algol-type system. In such semi-detached systems, it is known that the mass transfers from the evolved cool component to the hot primary component. The effects of this mass transfer can be seen in the photometric and spectroscopic data. Therefore, we traced the signature of mass transfer especially in the spectra of TZ Dra. It turned out that Hα lines show quite different structures which allowed us to confirm the mass transfer. As a result of the Hα line examination, we found that there is an emission line that is caused by the star-stream or star-disk interaction between both binary components. Additionally, it was obtained that there is a stream projected against the hot component. Furthermore, in the binary modelling, we also found a hot spot on the primary star's surface. That is both quite interesting because there is a little number of Algol systems having a hot spot and also remarkable situation.

To explain the mass-loss in Algol-type systems there are four different mechanisms, bipolar jets (Umana et al. 2000; Umana, Leone, & Trigilio 2002), mass-loss from 3rd Lagrangian point (Sytov et al. 2007), winds (Maeder & Stahler 2009) and the presence of a hot spot (Deschamps et al. 2013, 2015). The hot spot mechanism seems to be the more suitable and convincing mechanism to explain mass loss from Algols. According to the hotspot model, the mass should be ejected from the primary star's surface via the radiation pressure of the hotspot (van Rensbergen et al. 2011; Deschamps et al. 2013, 2015). To reveal possible mass loss from the system an orbital period variation analysis was performed as well. In conclusion, a decrease in the orbital

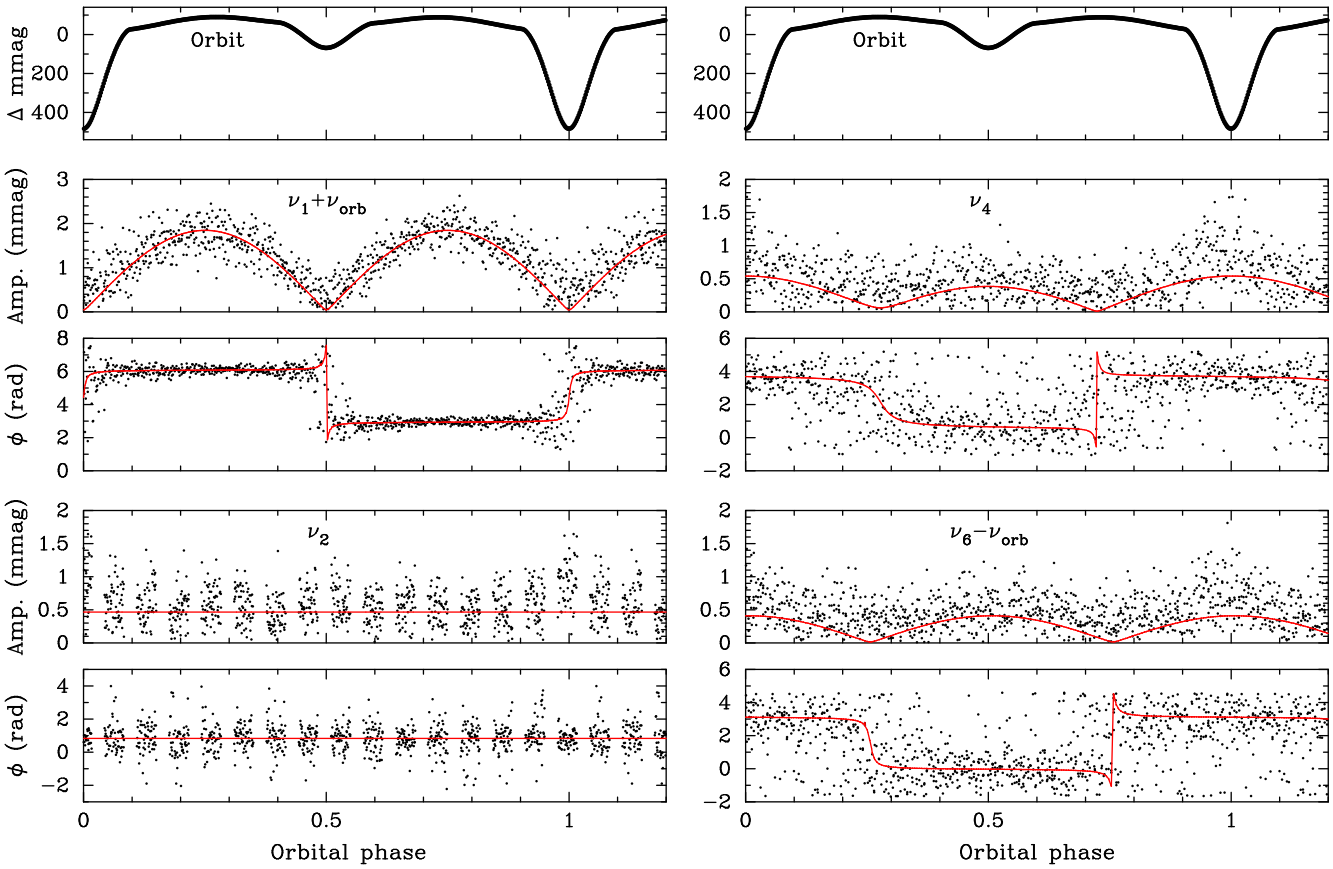

Figure 12. The run of the pulsation amplitudes and phases of four selected modes of TZ Dra over the orbital cycle (bottom four panels left and right). The black dots are individual determinations, the red lines are fits using the signal parameters from Table 6. Top: binary-induced light curve.

period was obtained and that could be explained with the mass loss by the hotspot and the winds in the secondary component. With this results, we showed that TZ Dra is a unique system to understand the mass transfer and the mass loss mechanism in Algol-type binaries.

The pulsation feature of the primary binary component was examined and thigh pulsation frequencies (i.e. p modes) ranging from 35.26 to 58.27 d^{-1} were found. During the analysis, it was found that significant amount of pulsation frequencies are spaced by the integer multiples of the orbital period and the star was shown to be a tidally tilted pulsator. According to the pulsation analysis we estimated that the star show high-order p modes in the range of second to fifth radial overtones.

TZ Dra is an interesting object for understanding the mass transfer and mass loss mechanism in Algol-type systems, as well as its impact on the pulsations. It is also usable for the theoretical modelling of mass transfer effect and/or mass loss effect on pulsations. With the combination of the results of the studies for similar systems, these effects can be interpreted more efficiently and help us improve the current knowledge about the Algol type pulsating systems.

ACKNOWLEDGMENTS

This study has been supported by the Scientific and Technological Research Council (TUBITAK) project through 120F330. GH thanks the Polish National Center for Science (NCN) for supporting the study through grant 2015/18/A/ST9/00578. IST60 telescope and its equipment are supported by the Republic of Turkey Office of Strategy and Budget with the project 2016K12137 and Istanbul University with the project numbers BAP-3685 and FBG-2017-23943. Based on observations made with the Mercator Telescope, operated on the island of La Palma by the Flemish Community, at the Spanish Observatorio del Roque de los Muchachos of the Instituto de Astrofisica de Canarias. This work has made use of data from the European Space Agency (ESA) mission Gaia (http://www.cosmos.esa.int/gaia), processed by the Gaia Data Processing and Analysis Consortium (DPAC, http://www.cosmos.esa.int/web/gaia/dpac/consortium). Funding for the DPAC has been provided by national institutions, in particular the institutions participating in the Gaia Multilateral Agreement. This research has made use of the SIMBAD data base, operated at CDS, Strasbourq, France.

DATA AVAILABILITY

The data underlying this work will be shared at reasonable requestto the corresponding author.

REFERENCES

Alfonso-Garzón J., Montesinos B., Moya A., Mas-Hesse J. M., Martín-Ruiz S., 2014, MNRAS, 443, 3022

Asplund M., Grevesse N., Sauval A. J., Scott P., 2009, ARA&A, 47, 481

Balona L. A., 2014, MNRAS, 439, 3453. doi:10.1093/mnras/stu193

Breger M., Stich J., Garrido R., Martin B., Jiang S.-Y., Li Z.-P., Hube D. P., et al., 1993, A&A, 271, 482

Catanzaro G., Leone F., Dall T. H., 2004, A&A, 425, 641

Deschamps R., Siess L., Davis P. J., Jorissen A., 2013, A&A, 557, A40. doi:10.1051/0004-6361/201321509

Deschamps R., Braun K., Jorissen A., Siess L., Baes M., Camps P., 2015, A&A, 577, A55. doi:10.1051/0004-6361/201424772

Dziembowski W., 1977, AcA, 27, 203

Erdem A., Aliçavuş F., Soydugan F., Doğru S. S., Soydugan E., Çiçek C., Demircan O., 2011, NewA, 16, 498. doi:10.1016/j.newast.2011.05.001

Faulkner D. R., 1986, PASP, 98, 690. doi:10.1086/131814

Fitch W. S., 1981, ApJ, 249, 218. doi:10.1086/159278

Fuller J., Kurtz D. W., Handler G., Rappaport S., 2020, MNRAS, 498, 5730. doi:10.1093/mnras/staa2376

Handler G., Kurtz D. W., Rappaport S. A., Saio H., Fuller J., Jones D., Guo Z., et al., 2020, NatAs, 4, 684. doi:10.1038/s41550-020-1035-1

Herbig G. H., 1960, ApJ, 131, 632. doi:10.1086/146876

Houdek G., Balmforth N. J., Christensen-Dalsgaard J., Gough D. O., 1999, A&A, 351, 582

Irwin J. B., 1959, AJ, 64, 149. doi:10.1086/107913

Kahraman Aliçavuş F., et al., 2016, MNRAS, 458, 2307

Kahraman Aliçavuş F., Soydugan E., Smalley B., Kubát J., 2017, MNRAS, 470, 915. doi:10.1093/mnras/stx1241

Kahraman Aliçavuş F and Aliçavuş F., 2020, MNRAS, 488, 5279

Kopal, Z., 1955, Annales d'Astrophysique, 18, 379

Kurtz D. W., Handler G., Rappaport S. A., Saio H., Fuller J., Jacobs T., Schmitt A., et al., 2020, MNRAS, 494, 5118. doi:10.1093/mnras/staa989

Kurucz R. L., Avrett E. H., 1981, SAOSR, 391,

Kurucz R., 1993, KurCD, 13,

Kreiner J. M., 2004, AcA, 54, 207

Kwee K. K., van Woerden H., 1956, BAN, 12, 327

Lampens P., 2021, Galax, 9, 28. doi:10.3390/galaxies9020028

Lenz P., Breger M., 2005, CoAst, 146, 53

Liakos A., Niarchos P., 2013, Ap&SS, 343, 123. doi:10.1007/s10509-012-1237-9

Liakos A., Niarchos P., 2017, MNRAS, 465, 1181. doi:10.1093/mnras/stw2756

Maeder A., Stahler S., 2009, PhT, 62, 52. doi:10.1063/1.3226770

Miszuda A., Szewczuk W., Daszyńska-Daszkiewicz J., 2021, MNRAS, 505, 3206. doi:10.1093/mnras/stab1597

Mkrtichian D. E., Kusakin A. V., Gamarova A. Y., Rodriguez E., Kim S. L., Kim C., Janiashvili E. B., et al., 2002, ASPC, 256, 259

Mkrtichian D. E., Kusakin A. V., Rodriguez E., Gamarova A. Y., Kim C., Kim S.-L., Lee J. W., et al., 2004, A&A, 419, 1015. doi:10.1051/0004-6361:20040095

Mkrtichian D. E., Rodríguez E., Olson E. C., Kusakin A. V., Kim S.-L., Lehmann H., Gamarova A. Y., et al., 2005, ASPC, 333, 197

Montgomery M. H., Odonoghue D., 1999, DSSN, 13

Pribulla T., Chochol D., Tremko J., Kreiner J. M., 2005, ASPC, 335, 103

Rappaport S. A., Kurtz D. W., Handler G., Jones D., Nelson L. A., Saio H., Fuller J., et al., 2021, MNRAS, 503, 254. doi:10.1093/mnras/stab336

Raskin G., et al., 2011, A&A, 526, A69

Reed M. D., Brondel B. J., Kawaler S. D., 2005, ApJ, 634, 602. doi:10.1086/491666

Ricker G. R., Winn J. N., Vanderspek R., Latham D. W., Bakos G. Á., Bean J. L., Berta-Thompson Z. K., et al., 2015, JATIS, 1, 014003. doi:10.1117/1.JATIS.1.1.014003

Rodríguez E., García J. M., Mkrtichian D. E., Costa V., Kim S.-L., López-González M. J., Hintz E., et al., 2004, MNRAS, 347, 1317. doi:10.1111/j.1365-2966.2004.07314.x

Ruciński S. M., 1969, AcA, 19, 245

Sana H., Evans C. J., 2011, IAUS, 272, 474

Smalley B., Gardiner R. B., Kupka F., Bessell M. S., 2002, A&A, 395, 601

Smalley B., 2005, MSAIS, 8, 130

Steindl T., Zwintz K., Bowman D. M., 2021, A&A, 645, A119. doi:10.1051/0004-6361/202039093

Sytov A. Y., Kaigorodov P. V., Bisikalo D. V., Kuznetsov O. A., Boyarchuk A. A., 2007, ARep, 51, 836. doi:10.1134/S1063772907100083

Soydugan E., Soydugan F., Demircan O., İbanoğlu C., 2006, MNRAS, 370, 2013. doi:10.1111/j.1365-2966.2006.10628.x

Soydugan F., Frasca A., Soydugan E., Catalano S., Demircan O., Ibanoğlu C., 2007, MNRAS, 379, 1533. doi:10.1111/j.1365-2966.2007.12065.x

Soydugan E., Tuysuz M., Bakıs V., Soydugan F., Senyuz T., Bilir S., Frasca A., et al., 2008, CoAst, 157, 379

Soydugan E., Soydugan F., Şenyüz T., Püsküllü Ç., Demircan O., 2011, NewA, 16, 72. doi:10.1016/j.newast.2010.08.003

Soydugan E., Soydugan F., Aliçavuş F., Erdem A., 2016, NewA, 46, 40. doi:10.1016/j.newast.2015.12.007

Stassun K. G., Oelkers R. J., Paegert M., Torres G., Pepper J., De Lee N., Collins K., et al., 2019, AJ, 158, 138. doi:10.3847/1538-3881/ab3467

Sumter G. C., Beaky M. M., 2007, IBVS, 5798, 1

Tempesti P., 1971, IBVS, 596, 1

Tody D., 1986, SPIE, 627, 733, SPIE..627

Umana G., Maxted P. F. L., Trigilio C., Fender R. P., Leone F., Yerli S. K., 2000, A&A, 358, 229

Umana G., Leone F., Trigilio C., 2002, A&A, 391, 609. doi:10.1051/0004-6361:20020878

van Hamme W., 1993, AJ, 106, 2096

van Rensbergen W., de Greve J. P., Mennekens N., Jansen K., de Loore C., 2011, A&A, 528, A16. doi:10.1051/0004-6361/201015596

Vesper D., Honeycutt K., Hunt T., 2001, AJ, 121, 2723. doi:10.1086/320381

von Zeipel H., 1924, MNRAS, 84, 665

Wilson R. E., Devinney E. J., 1971, ApJ, 166, 605

Zasche P., Liakos A., Niarchos P., Wolf M., Manimanis V., Gazeas K., 2009, NewA, 14, 121. doi:10.1016/j.newast.2008.06.002

Zola S., et al., 2004, AcA, 54, 299

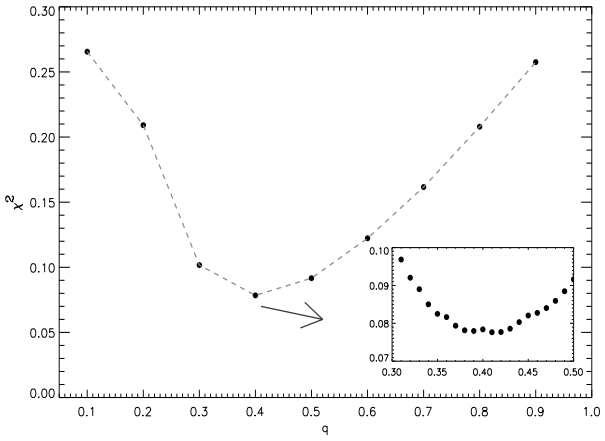

Figure A1. q search for TZ Dra.

Zola S., Gazeas K., Kreiner J. M., Ogloza W., Siwak M., Koziel-Wierzbowska D., Winiarski M., 2010, MNRAS, 408, 464

Appendix

Table A1. The v_r measurements.

HJD (2450000+)	v_r (km s^{-1})
8986.6784	-90.041 ± 0.327
8988.5584	-11.297 ± 0.331
8990.6811	-48.080 ± 0.421
8996.6396	25.589 ± 0.472
9052.5008	-84.507 ± 0.377
9052.5166	-67.123 ± 0.357
9052.5324	-60.867 ± 0.511
9053.4981	3.202 ± 0.513
9053.5140	13.055 ± 0.314
9053.5297	18.949 ± 0.331
9053.5453	27.319 ± 0.327
9054.4748	59.870 ± 1.516
9054.5025	65.697 ± 1.313
9054.5180	66.848 ± 1.321
9054.5550	62.872 ± 1.490
9054.5611	61.067 ± 1.358
9055.5291	30.682 ± 0.500
9055.5446	18.770 ± 0.571
9055.5626	13.521 ± 0.536
9055.5780	8.488 ± 0.456
9055.5936	0.392 ± 0.492
9056.4432	11.107 ± 0.552
9058.4698	-111.006 ± 1.289
9059.4628	-56.888 ± 0.607
9060.4460	13.703 ± 0.637
9090.4743	-111.172 ± 0.503
9093.3841	33.861 ± 1.110
9093.3999	40.637 ± 1.308
9093.4154	46.740 ± 0.868
9093.4310	54.564 ± 0.921
9094.3956	67.568 ± 1.313
9094.4113	62.270 ± 1.219
9094.4269	60.672 ± 1.153
9096.3645	-49.920 ± 0.682
9096.3803	-55.208 ± 0.387
9096.3960	-61.628 ± 0.546

Table A2. The minima times derived from the TESS data and our photometric observation in V and R filter. I and II repsresent the primary and secondary minimums. For the V,R photomteric observation a median minima time is given.

Time of minima HJD (2450000+)	Filter	Minima type
8983.74370 ± 0.00003	TESS	I
8985.47575 ± 0.00002	TESS	I
9008.85843 ± 0.00003	TESS	I
8984.17794 ± 0.00011	TESS	II
8985.04381 ± 0.00020	TESS	II
9003.23004 ± 0.00008	TESS	II
9010.59182 ± 0.00003	TESS	I
9025.31420 ± 0.00004	TESS	I
9032.24248 ± 0.00003	TESS	I
9011.89158 ± 0.00010	TESS	II
9025.74788 ± 0.00009	TESS	II
9032.67621 ± 0.00009	TESS	II
9405.49803 ± 0.00029	VR	I